Computers & Geosciences 77 (2015) 54–65

Contents lists available at ScienceDirect

Computers & Geosciences

journal homepage: www.elsevier.com/locate/cageo

Reconstruction of channelized geological facies based on RIPless compressed sensing

Hernán Calderón [a,c], Jorge F. Silva [a,c,*], Julián M. Ortiz [b,c], Alvaro Egaña [b,c]

[a] Department of Electrical Engineering, University of Chile, Av. Tupper 2007, Santiago 837-0451, Chile
[b] Department of Mining Engineering, University of Chile, Av. Tupper 2069, Santiago 837-0451, Chile
[c] Advanced Mining Technology Center (AMTC), University of Chile, Chile

ARTICLE INFO

Article history:
Received 13 June 2014
Received in revised form
2 October 2014
Accepted 12 January 2015
Available online 14 January 2015

Keywords:
Multichannel facies images
Compressed sensing
Basis selection
Discrete cosine transform

ABSTRACT

This work proposes a new approach for multichannel facies image reconstruction based on compressed sensing where the image is recovered from pixel-based measurements without the use of prior information from a training image. An l_1– minimization reconstruction algorithm is proposed, and a performance guaranteed result is adopted to evaluate its reconstruction. From this analysis, we formulate the problem of basis selection, where it is shown that for unstructured pixel-based measurements the Discrete Cosine Transform is the best choice for the problem. In the experimental side, signal-to-noise ratios and similarity perceptual indicators are used to evaluate the quality of the reconstructions, and promising reconstruction results are obtained. The potential of this new approach is demonstrated in under-sampled scenario of 2–4% of direct data, which is known to be very challenging in the absence of prior knowledge from a training image.

1. Introduction

The reconstruction of images from scarce measurements is the essence of many inverse problems in Geosciences. Direct measurements are expensive and an exhaustive analysis is out of the possibilities. In this sampling context, the conventional way to treat the lack of data in geostatistics has been by incorporating prior information of a statistical model that captures the geological structure a family of images (Mariethoz and Renard, 2010; Ortiz and Deutsch, 2004). On this, the use of non-parametric models for statistical simulation is a well-established approach (Ortiz and Deutsch, 2004). Among these methods, multiple-point (MP) simulation techniques are widely used for the reconstruction of geological structures (Guardiano and Srivastava, 1993; Strebelle, 2002; Arpat and Caers, 2007; Wu et al., 2008). These approaches use a small portion of wells (direct measurements in the pixel domain) to recover a collection of images by means of reproducing the statistical patterns of the selected model. This is a stochastic approach where the variability in the results is intrinsic and, consequently, it does not lead to a single representation of the distribution of facies.

This work departs from the problem of image recovery based on reproducing patterns of a training image (Ortiz and Deutsch, 2004; Tahmasebi et al., 2014; Mariethoz and Renard, 2010; Mariethoz and Lefebvre, 2014), and treats the image recovery as a generalized sampling problem (Vetterli and Kovacevic, 1995; Donoho et al., 1998; Mallat, 2009). We follow the essential idea proposed by Jafarpour and McLaughlin (2009), Jafarpour et al. (2009, 2010), Jafarpour (2011) in the context of subsurface flow model characterization from nonlinear measurements (Khaninezhad et al., 2012; Elsheikh et al., 2013; Khaninezhad and Jafarpour, 2014), which considers that subsurface facies images have a common structure that can be efficiently represented in a transform domain. Then, our conjecture is that this signal structure is information that can be used to recover the missing pixels directly from the partial measurements. To validate this, we propose to study the compressible structure of the facies and with this the critical rate of measurements needed to achieve a given reconstruction quality.

In the setting of image reconstruction (Donoho et al., 1998; Vetterli and Kovacevic, 1995; Elad, 2010), the figure of merit is a comparison of the recovered image with the true image using distortion measures like the signal to noise ratio (SNR) or visual perceptual indicators (Zhou et al., 2004). In contrast, the conventional way of evaluating the quality of geostatistic simulations has been based on assessing the reproduction of univariate, bivariate and multiple-point statistics of an image model (Ortiz and Deutsch, 2004; Mariethoz and Renard, 2010; Tan et al., 2014;

* Corresponding author at: Department of Electrical Engineering, University of Chile, Av. Tupper 2007, Santiago 837-0451, Chile. Fax: +56 2 6953881.
E-mail addresses: hcaldero@ing.uchile.cl (H. Calderón), jorgesil.edu@gmail.com, josilva@ing.uchile.cl (J.F. Silva), jortiz@ing.uchile.cl (J.M. Ortiz), aegana@alges.cl (A. Egaña).
URL: http://www.ids.uchile.cl/~josilva/ (J.F. Silva).

http://dx.doi.org/10.1016/j.cageo.2015.01.006
0098-3004/

Peredo and Ortiz, 2011; Leuangthong et al., 2004). Therefore, in the sampling-reconstruction context of this work, we move the attention to the more challenging objective of true image recovery from a small fraction of its pixels. Under this umbrella, this work focus on the extension of the framework of compressed sensing to the context of facies image reconstruction from pixel-based measurements.

Compressed sensing (CS) has introduced a new paradigm for the classical problem of sensing and reconstruction (Candès and Tao, 2005, 2006; Candès et al., 2006a,b; Donoho, 2006). In a nutshell, the idea of CS is to model signals that are embedded in a small sub-dimension of a target space, and to capture that information using the fewest possible measurements. The structure of an image is measured by notions of sparseness and compressibility, which is the ability of the image to be perfect or well approximated by its best k-sparse version. Sources like natural images and acoustic signals are emblematic examples of this notion of compressibility (Mallat, 2009; Vetterli and Kovacevic, 1995). On the theoretical side, the main CS results offer conditions for perfect reconstruction under a number of measurements (Candès et al., 2006b; Donoho, 2006), which are far below the classical Nyquist–Shannon sampling rate (Nyquist, 1928; Shannon, 1949). In the practical side, there are well-documented algorithms to solve the recovery problem based on linear programming as well as greedy iterative solutions (Mallat and Zhang, 1993; Tropp and Gilbert, 2007; Blumensath and Davies, 2009; Elad, 2010).

The application of CS to inverse problems in geosciences is an active area of research. In particular, several contributions have been developed in the problem of subsurface flow model calibrations based on non-linear flow measurements (Jafarpour et al., 2010; Jafarpour, 2011; Khaninezhad et al., 2012; Elsheikh et al., 2013; Khaninezhad and Jafarpour, 2014; Lee and Kitanidis, 2013). In these contributions, CS results are used to propose new sparsity promoting algorithms that recover subsurface models based on the formulation of complexity regularization problem. These scenarios are estimation problems based on complex nonlinear (flow) measurements and do not belong to the category of sampling problems explored in this work. In addition, CS has also been applied to other relevant inverse problems in geophysics (Herrmann and Li, 2012; Herrmann et al., 2012).

For the specific context of recovering a channelized facies image from pixel-based measurements, the work of Jafarpour et al. (2009) is the first that explored the role of CS. They focused on the analysis of a mono-channel image model and a specific data-rate regime, where promising results were obtained. In this work we extend this direction in a number of new dimensions: addressing the formal connections with the RIPless theory of CS, exploring and formulating the problem of basis selection, proposing variations of the classical basis pursuit algorithm, proposing an inter-block approach for processing arbitrary large images, and finally, conducting a systematic experimental analysis to validate the approach in different data-rate regimes and scenarios.

We first formulate the image reconstruction problem as an instance of a CS reconstruction and establish concrete connections with the performance guarantee result of the *RIPless theory of CS*. As part of the formulation, the role of change of basis is analyzed and the problem of basis selection is addressed, where a concrete indicator to evaluate the quality of the basis in this transform-based framework is proposed. In particular, for our scenario of unstructured pixel-based measurements, the DCT shows the best performance in the sense of offering the best tradeoff between a reconstruction error and the number of measurements.

Applying the CS technique to the reconstruction of facies with the selected DCT basis, the regime from 1% to 10% of pixel measurements is explored. Promising results are shown even in the under-sample regime (from 2% to 4%) where the hard-data offers very limited contextual information. From these results, we can ratify that the underlying transform-based structure of channelized facies images is very rich, and that the CS offers an effective solution to recover that image from very limited and unstructured pixel-based data. Our results are evaluated in terms of concrete performances versus rate of measurements curves, which resolves the question of the critical number of measurements that is needed to achieve a given level of image reconstruction. Furthermore, a novel post-processing stage is proposed that considers averaging information across different block-by-block reconstructions and a final hard-thresholding process to pass from continuous to categorical values. This final stage is systematically evaluated and offers a relevant performance boost in the critical regime from 2% to 10% of the pixel data.

1.1. Problem formulation

Our problem is the recovery of a geological structure from the acquisition of vertical wells. More precisely, we focus on the family of 2D facies distributions over a deposit or reservoir as illustrated in Fig. 1(a). This problem is modeled as the recovery of an image (a collection of pixels $(x_{i,j}) \in \mathbb{R}^{\{1,\dots,N\}\times\{1,\dots,N\}}$ indexed by the pair $(i, j) \in \{1, \dots, N\} \times \{1, \dots, N\}$), where the wells correspond to unstructured pixel measurements of a small proportion of the image size in the range [1%, 10%], see Fig. 1(b). In this drastic under-sampling regime, any classical interpolation or sampling technique offers poor performance. Then, the use of prior knowledge of the image is mandatory to achieve a reasonable recovery from the limited information in Fig. 1(b).

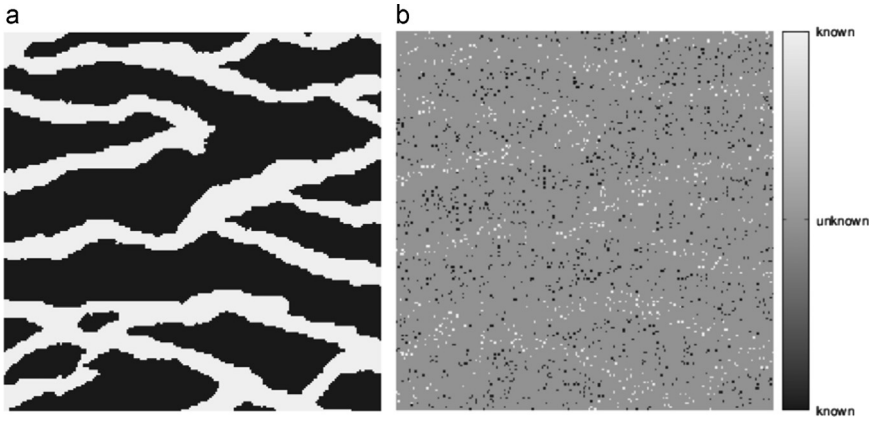

Fig. 1. (a) A multichannel facies image. (b) Unstructured pixel-based measurements (5% taken at random positions). Gray pixels indicate the absence of the measurement.

The next section is devoted to provide a concise presentation of the CS approach adopted in this work, as well as its performance guarantee. With this background, in Section 3 we add the needed operational restrictions and considerations that allow us to state the main recovery result of our problem. The main reason to present this formality is two folds: first to concretely understand the role of the basis in this reconstruction problem, and second, to characterize an objective function that allows us to address the problem of basis selection. This last problem is elaborated in Sections 4 and 5. Finally, Section 6 provides the experimental results for geological facies reconstruction, and Section 7 presents final remarks and discussion on future work.

2. Elements of CS

We model an image as a finite dimensional vector x in $\mathbb{R}^n$. On this context, our sensing modality is a linear operator, i.e.,

$$y = Ax \in \mathbb{R}^m \tag{1}$$

where A is an m by n matrix and y denotes the observation vector. Here we focus on the under sampling regime $m < n$, where the recovery of x from y is an ill-posed problem. However under specific conditions on x, the CS theory tells us that it is possible to obtain perfect reconstruction (Candès and Tao, 2005; Candès et al., 2006b; Donoho, 2006; Cohen et al., 2009). We elaborate this over *the RIPless theory of CS* (Candès and Plan, 2011).

This theory is constructed over a sensing modality that is random. More formally, the m-rows of the matrix A, i.e., $\{a_k: k = 1, \ldots, m\} \subset \mathbb{R}^n$ are generated from independent and identically distributed (i.i.d.) realizations of a random vector in $\mathbb{R}^n$ with a probability that we denote by ρ (Candès and Plan, 2011). Another key concept is the notion of signal sparseness (Candès et al., 2006b; Donoho, 2006; Candès and Plan, 2011). A signal $x \in \mathbb{R}^n$ is said to be s-sparse, with $s \leq n$, if it has at most s coefficients different than zero. The collection of s-sparse signals is denoted by $\Sigma_s \subset \mathbb{R}^n$. For all $x \in \mathbb{R}^n$,

$$\sigma_s(x)_{l_p} \equiv \min_{\tilde{x} \in \Sigma_s} \|x - \tilde{x}\|_{l_p} \tag{2}$$

is the error of the best s-term approximation of x, where $\|x\|_p = (\sum_{i=1}^n |x_i|^p)^{1/p}$ is the p-norm with $p \geq 1$. Before we state the main CS result, we need to introduce two concepts:

Definition 1 (*Candès and Plan, 2011*). If the rows of A in (1) are i.i.d. realizations of a random vector $a(w)$ (with probability ρ), then A obeys the *isotropy* property if

$$\mathbb{E}_{a \sim \rho}(aa^\dagger) = I. \tag{3}$$

In addition, we define its *coherence* μ, as the smallest number such that if $a(w) = (a(w, 1), \ldots, a(w, n))^\dagger$ then

$$\max_{i=1,\ldots,n} |a(w, i)|^2 \leq \mu, \tag{4}$$

with probability 1.

Theorem 1 (*Candès and Plan, 2011, Theorem 1.2*). *Let $x \in \mathbb{R}^n$ and let us consider the linear acquisition model of Eq. (1), and the recovery algorithm given by the solution of the ℓ_1-minimization problem:*

$$\hat{x} = \arg \min_{\tilde{x} \in \mathbb{R}^n} \|\tilde{x}\|_{l_1} \quad \text{subject to } A\tilde{x} = y. \tag{5}$$

Then for any $s < n$ (level of sparsity) and $\beta > 0$, with probability (over the sensing matrix) $1 - 6/n - 6e^{-\beta}$, the solution to Eq. (5) satisfies that

$$\|\hat{x} - x\|_{l_2} \leq \frac{C(1+\alpha)}{\sqrt{s}} \cdot \sigma_s(x)_{l_1}, \tag{6}$$

provided that Eq. (3) is satisfied and

$$m \geq C_\beta \cdot \mu \cdot s \cdot \log n, \tag{7}$$

with $\alpha = \sqrt{(1+\beta) s\mu \log n \log m \log^2 s/m}$, $C_\beta = (1+\beta)C_0$, and C and C_0 numerical constants.

This result guarantees for m (number of measurements) of the order of $O(s \cdot \mu \log n)$, a perfect recovery of any sparse signal in $x \in \Sigma_s$ (as in this case $\sigma_s(x)_{l_1} = 0$ in Eq. (6)) adopting the ℓ_1-minimization decoder in Eq. (5). Then, the signal sparseness $(\sigma_s(x)_{l_1}$ in Eq. (6)), and the coherence coefficient μ (because of its role in Eq. (7)) are the two key design variables to achieve good-perfect performance in this CS setting.

3. Image reconstruction from random pixel measurements as a CS problem

There are two aspects of our image reconstruction problem that we need to model to reduce it to the CS setting in Section 2. First, facies images are no-sparse neither compressible in the coordinate domain, but instead they can be compressed in a transform domain (Vetterli and Kovacevic, 1995; Starck et al., 2010; Mallat, 2009). Second, we consider measurements taken at random pixel locations to model the sensing mechanics presented in Section 1.1. This random pixel location is a reasonable assumption as we consider that wells are taken in an unstructured way (i.e. we want to recover the 2D geological pattern universally among a family of images), although one could argue that they are placed using some prior knowledge of the geological structure of the deposit or reservoir.

Formally, let U be an unitary matrix, i.e., the columns of U define an orthonormal basis for $\mathbb{R}^n$, where the signal $x \in \mathbb{R}^n$ can be expressed by

$$x = Uz \tag{8}$$

with $z = U^\dagger x$ denoting the transform representation of x. Our pixel-based random sensing scheme is represented by $\tilde{a}(w)$, which independently takes m -columns of the identity matrix I with uniform probability to form the m-rows of a sensing matrix that we denote by $\tilde{A}$. Hence, (1) in our problem can be expressed as

$$y = \underbrace{\sqrt{n} \cdot \tilde{A}U}_{=A} \cdot z \in \mathbb{R}^m \tag{9}$$

relating the pixel-based measurements $y \in \mathbb{R}^m$ with $z \in \mathbb{R}^n$, which is the transform representation of the signal with respect to U. From this, it is simple to verify that $\mathbb{E}(aa^\dagger) = I$ for any basis U, and then the isotropy property in Definition 1 is satisfied.[1] Furthermore, we can state a version of Theorem 1 for our pixel-based imaging problem.

Corollary 1. *Let us consider $x \in \mathbb{R}^n$, the linear acquisition model in (9), and the recovery algorithm (in the transform domain) given by*

$$\hat{z} = \arg \min_{\tilde{z} \in \mathbb{R}^n} \|\tilde{z}\|_{l_1} \quad \text{subject to } y = A\tilde{z} = \sqrt{n}\tilde{A}U\tilde{z}. \tag{10}$$

Let us consider $s < n$ and $\beta > 0$, then with probability $1 - 6/n - 6e^{-\beta}$, the solution to Eq. (10) satisfies that

$$\|\hat{x} - x\|_{l_2} \leq \frac{C(1+\alpha)}{\sqrt{s}} \cdot \sigma_s(z)_{l_1}, \tag{11}$$

[1] The $\sqrt{n}$ terms in the RHS of (9) are needed to satisfy $\mathbb{E}(aa^\dagger) = I$.

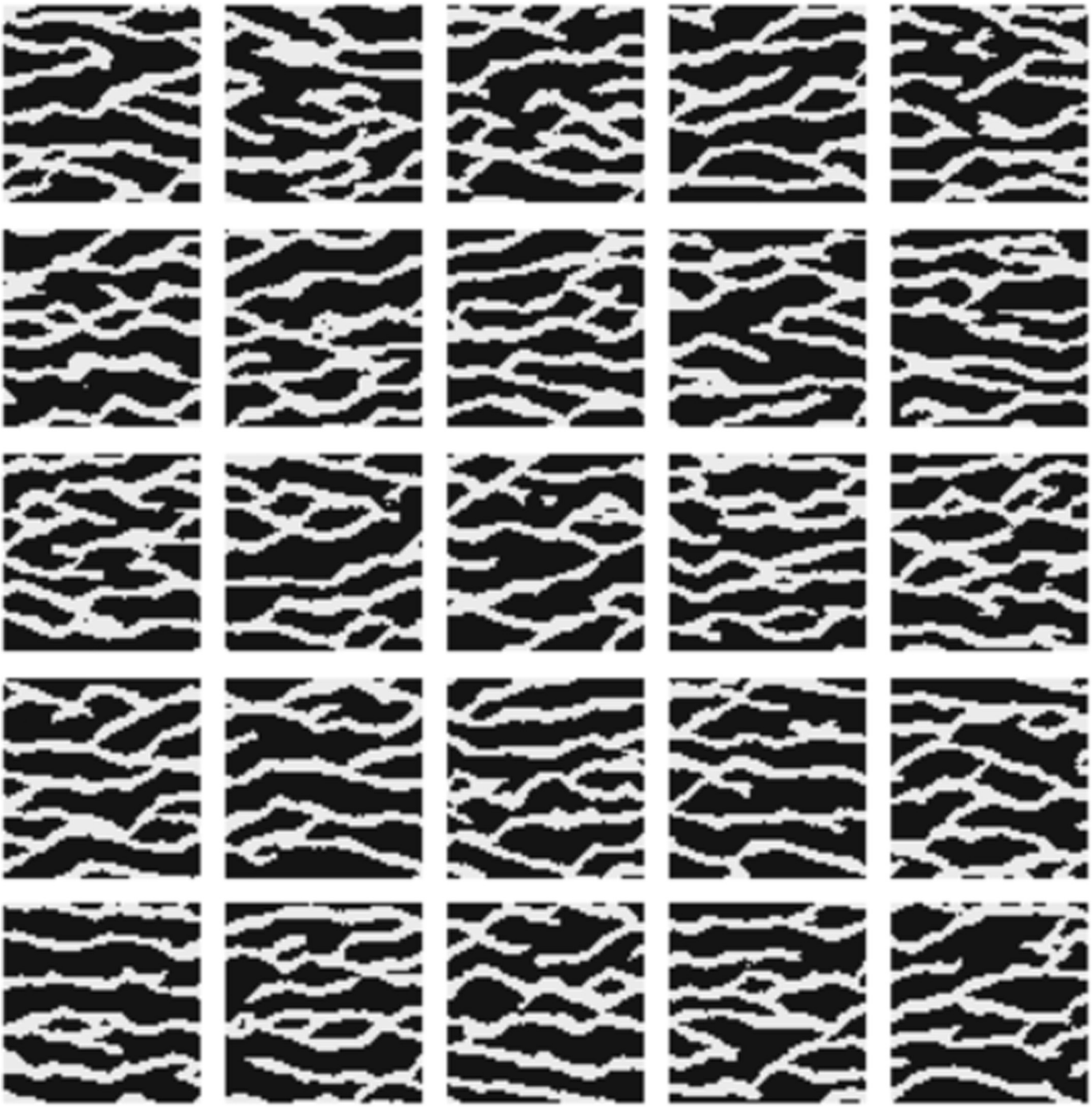

Fig. 2. A sample of the generated 2D multi-channel images used for analysis and reconstruction.

being $x = Uz$ *and* $\hat{x} = U\hat{z}$ *provided that* $m \geq C_\beta \cdot \mu(U) s \log n$. *In this case*

$$\mu(U) = n \cdot \max_{i,j \in \{1,\ldots,n\}} |u_{i,j}|^2 \tag{12}$$

is the coherence *of the sensing matrix in* (4), *where* $u_{i,j}$ *denotes the* i, j *entry of the unitary matrix* U.

3.1. Interpretation of Corollary 1

There are two important aspects about the role of the basis U in Corollary 1. First, $\sigma_s(z)_{l1}$, in Eq. (11), is an indicator of the quality of the basis U to represent x in few transform coefficients. Second, we have the critical condition

$$m \geq C_\beta \cdot \mu(U) s \cdot \log n \tag{13}$$

that says that the smaller the $\mu(U)$ is, the better the CS scheme performs, in terms of the number of measurements needed to achieve a given reconstruction error. Therefore, both the compressibility of the signal (after projection on U) and the coherence coefficients $\mu(U)$ play a key role to achieve good reconstruction.

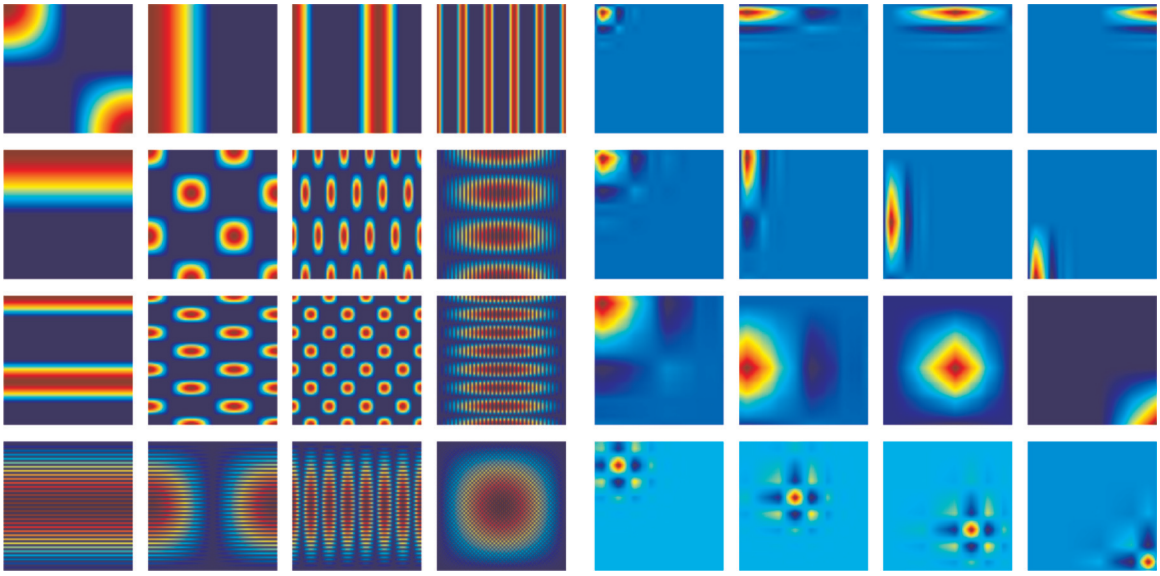

Fig. 3. The first 4 columns correspond to elements of the DCT basis and the last 4 columns correspond to elements of the Wavelet basis (Daubechies of order 3 with 5 levels of iteration).

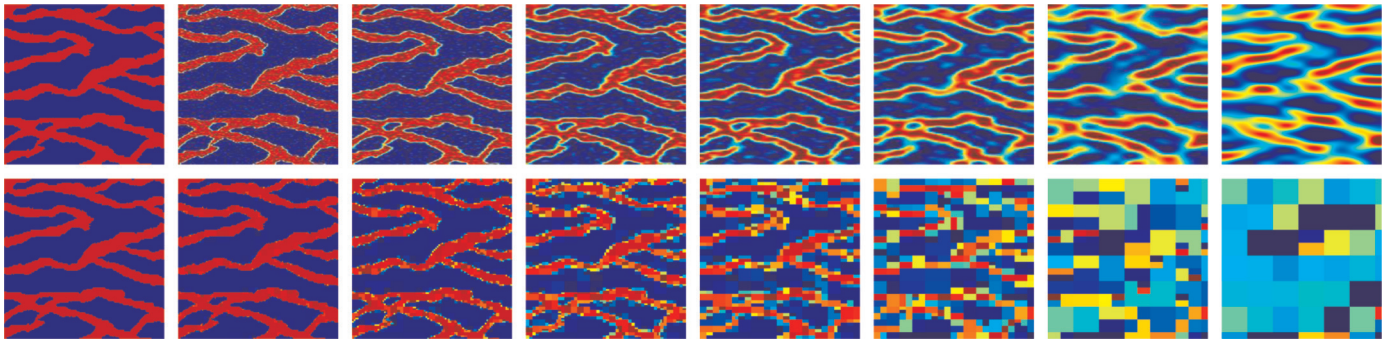

Fig. 4. Best k-term sparse approximation for the multichannel image using the DCT basis (first row) and the Haar basis with 5 levels of iteration (second row). From left to right: 100%, 10%, 5%, 2%, 1% 0.5% and 0.1% of more significant transform coefficients.

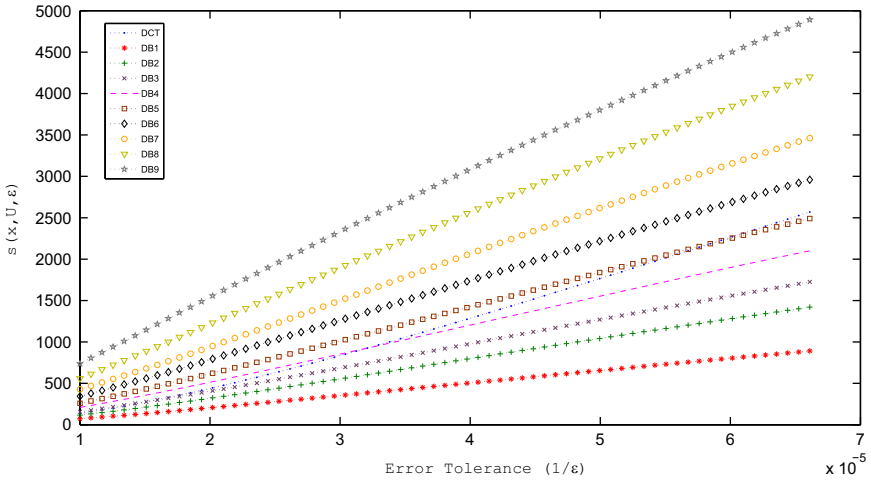

Fig. 5. Evolution of the ϵ-critical number of coefficients in Eq. (14) for the facies image in Fig. 4(a) function of $1/\epsilon$ and for different bases. DCT refers to the discrete cosine transform and DBx refers to the wavelet basis induced by the Daubechies two channel filer of order x with 5 levels of iteration.

4. Basis selection: a joint compressibility and incoherence analysis

Our key performance result in Corollary 1 is valid for every basis U. This offers a design variable and rises the problem of basis selection. Here we propose a formal methodology to address this problem.

For a basis U, a signal x, and a target reconstruction error $\epsilon > 0$, let us introduce the following concept:

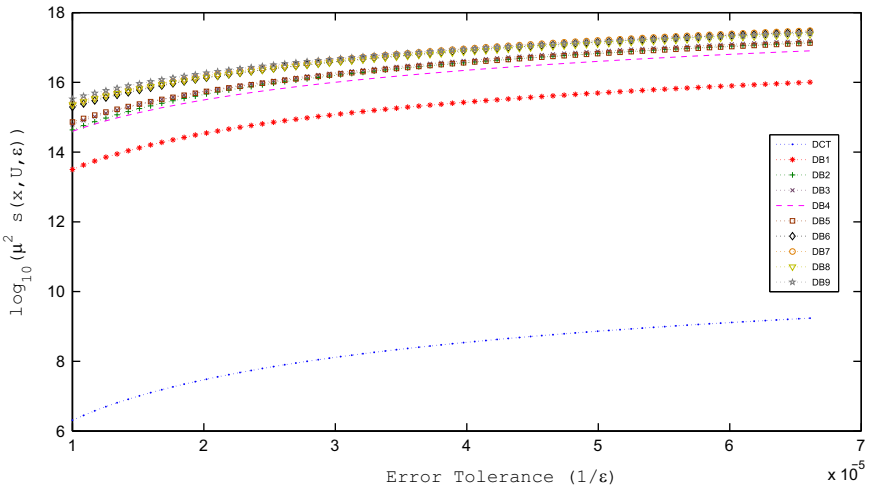

Fig. 6. Evolution of $s(x, U_j, \epsilon)\cdot\mu(U_j)^2$ in the RHS of Eq. (15) for the facies image in Fig. 7(a). Curves are generated for every bases (Wavelets and the DCT) as a function of the fidelity indicator $1/\epsilon$. For the Wavelet bases, the Daubechies two-channel filters of different orders are used, from DB1 to DB9.

Table 1
Coherence indicator for the DCT and Wavelet bases induced by the Daubechies two channel filers (DB) of different orders (from 1 to 9) and with 5 levels of iteration.

	DCT	Daubechies wavelet bases					
		Db1 (Haar)	Db2	Db3	Db5	Db7	Db9
$\sqrt{\mu(U_j)}$	2.00	100.00	139.95	130.21	104.92	106.33	86.41

$$s(x, U, \epsilon) \equiv \min\left\{1 \le s \le n\text{: such that } \frac{C(1+\alpha)}{\sqrt{s}}\cdot\sigma_s(U^\dagger x)_{l1} \le \epsilon\right\}, \tag{14}$$

which is the *critical number of the significant transform coefficients* needed to have a reconstruction error smaller than ϵ. Equipped with this notion, if we have a collection of bases $\{U_j: j \in J\}$, from Eq. (13) we can choose the basis that offers the smallest lower bound on the number of random-pixel measurements as the solution of

$$j^*(\epsilon, x) = \arg\min_{j\in J} s(x, U_j, \epsilon)\cdot\mu(U_j). \tag{15}$$

This solves the problem of basis selection from the point of view of minimizing the number of measurements, where $j^*(\epsilon, x)$ finds an optimal balance between compressibility, in terms of $s(x, U_j, \epsilon)$ in (14), and coherence, in terms of $\mu(U_j)$ in (12).

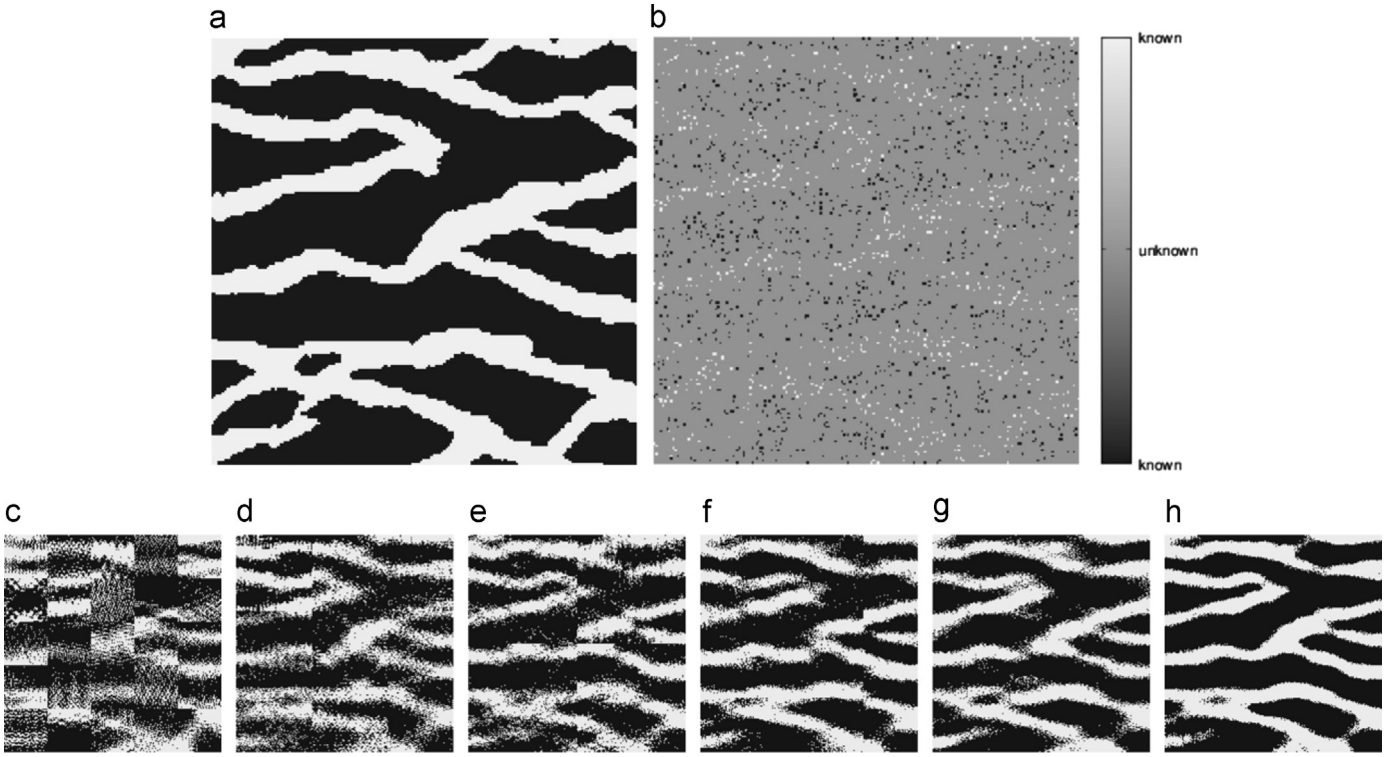

Fig. 7. CS reconstructions obtained with 4% of random pixel measurements. (a) Original multichannel image. (b) Random pixel measurements. (c) Reconstruction obtained by processing sub-images with block size of 40 × 40 pp. (d) Reconstruction with blocks of 70 × 70 pp. (e) Reconstruction with blocks of 100 × 100 pp. (f) Reconstruction with blocks of 150 × 150 pp. (g) Reconstruction with blocks of 200 × 200 pp. (h) Reconstruction obtained by averaging (block-by-block reconstructions from 40 × 40 pp to 200 × 200 pp) and thresholding pixel by pixel information.

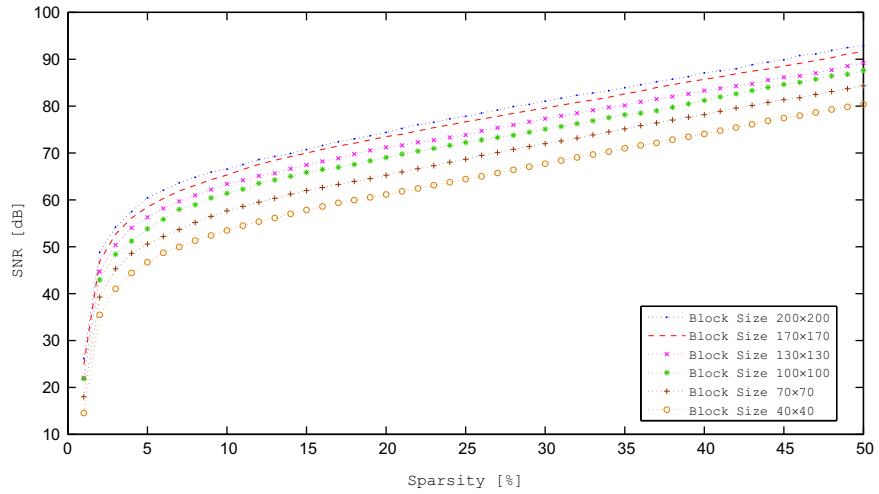

Fig. 8. Approximation errors measured in terms of $10 \log \|x\|_2/\sigma_s(x)_{l2}$, i.e., signal to noise ratio (SNR) in dB, for the image presented in Fig. 7. The SNR curves are presented across the number of significant coefficients, and for different block sizes of the image.

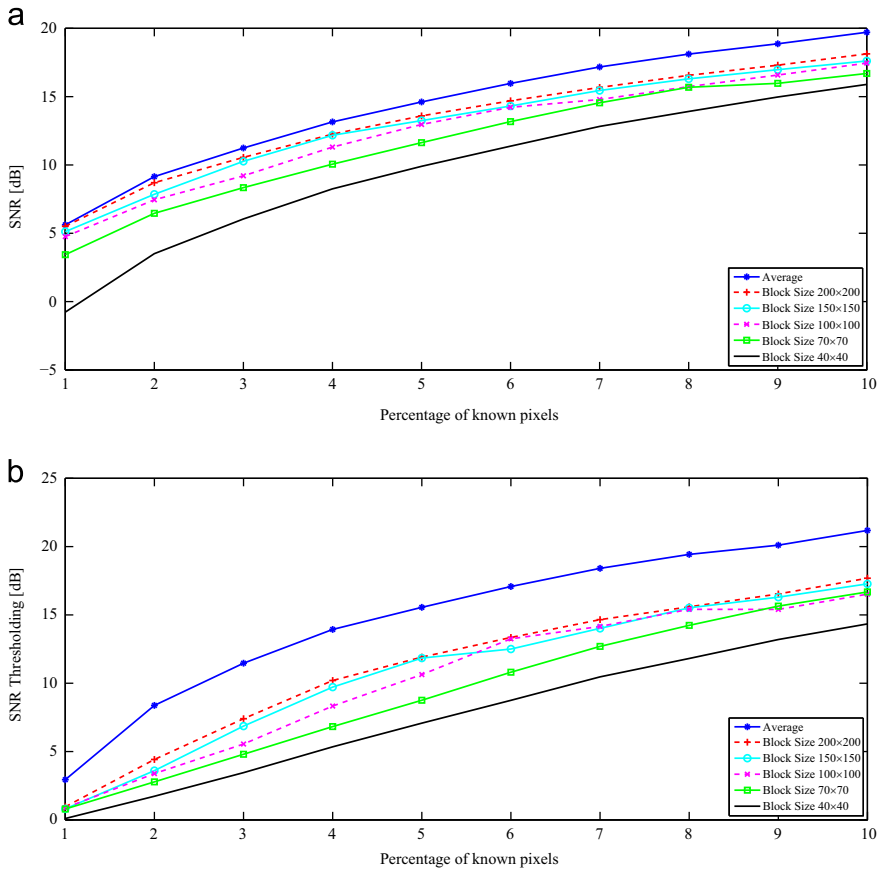

Fig. 9. Performances of the image reconstruction as a function of the number of pixel-based measurements and the block-size in the proposed block-by-block CS reconstruction scheme. Performances are measured in terms of the signal to noise ratio in decibels (dB). (a) shows the original results, (b) shows the results after thresholding.

5. Analysis for the problem of facies field reconstruction

The focus of this section is to present the bases considered on the analysis of facies images, as well as to solve (15) in this context. Examples of these 2D multichannel structures are presented in Fig. 2. For the bases, we consider the collection of wavelets induced by the *Daubechies* two channel filters (Db) (Vetterli and Kovacevic, 1995; Daubechies, 1988) of different orders (from 1 to 9) and number of iterations (from 1 to 5), as well as the widely adopted *discrete cosine transform* (DCT) (Jafarpour and McLaughlin, 2009). Some examples of the elements of these bases are presented in Fig. 3.

Moving to the basis selection, first Fig. 5 shows the ϵ-critical number of coefficients in Eq. (14) of a typical field (the image in Fig. 4) as a function of $1/\epsilon$ and for our family of bases (DCT and Wavelets). Here, it is clear that wavelet bases of smaller order offer better representations than the DCT in terms of critical number of coefficients across a wide range of fidelity values $1/\epsilon$. In particular, the solution of the smallest order (DB1) or the *Haar Wavelet* (Vetterli and Kovacevic, 1995) has the best performance as it

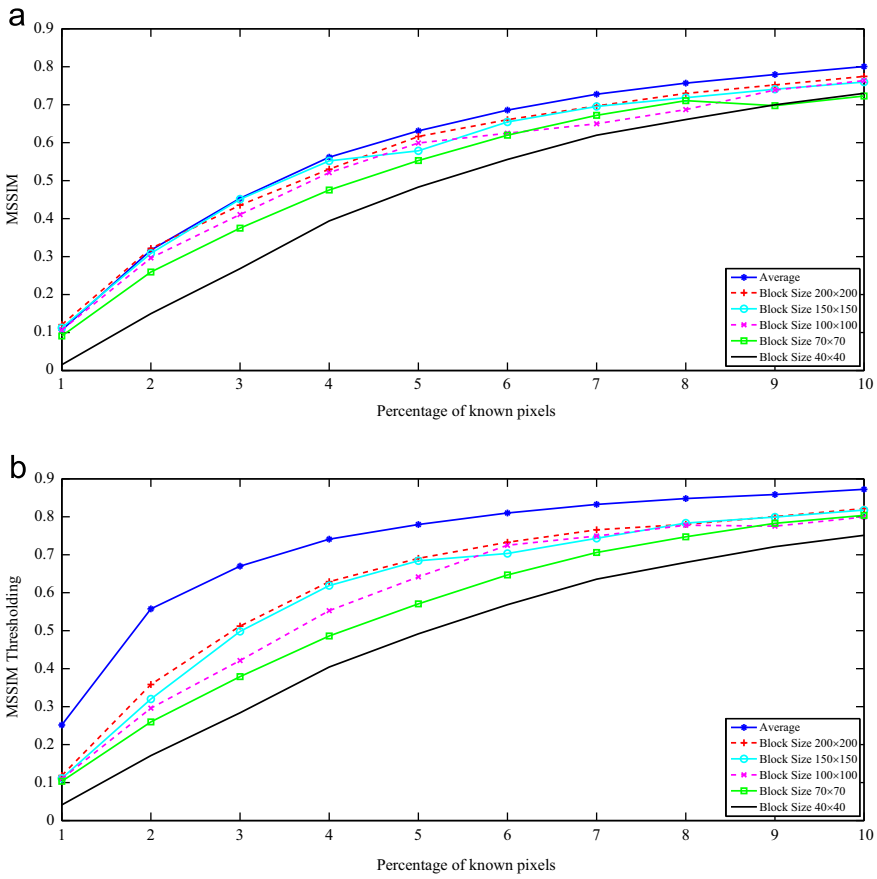

Fig. 10. Same as caption of Fig. 9. Performance is measured in terms of the structure similarity index (SSIM).

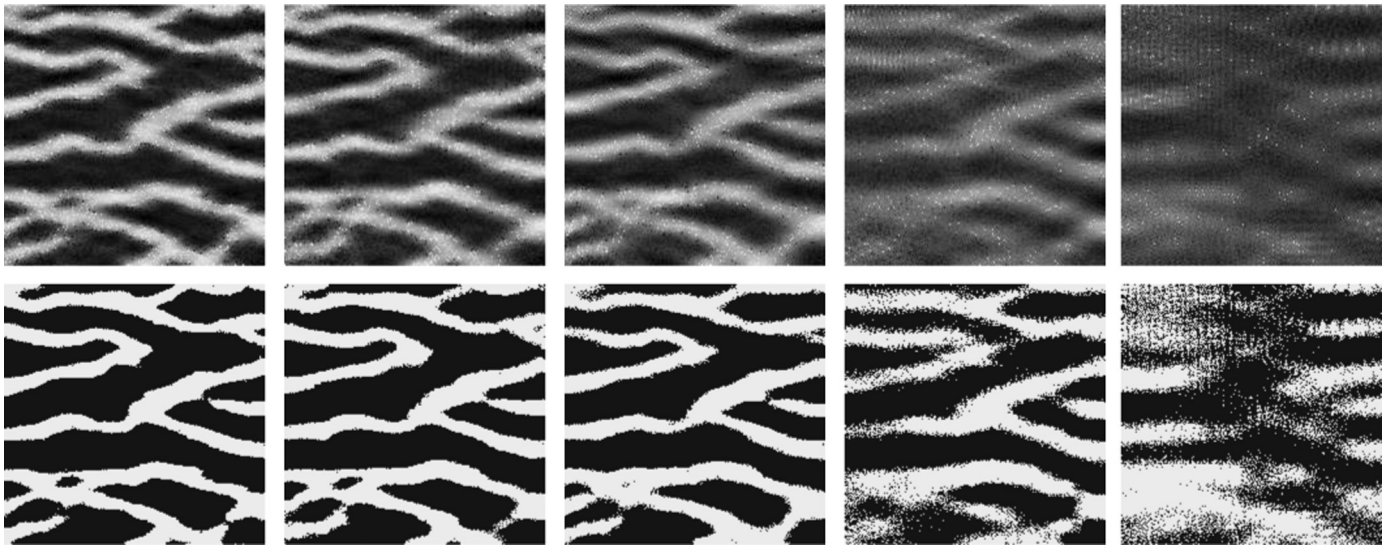

Fig. 11. Reconstructions using the adaptive hard-thresholding stage. The first row shows average reconstructions across block sizes without hard-thresholding, and the second row shows the respective results with the hard-thresholding. From left to right in columns: 10%, 7%, 5%, 2% and 1% of direct data.

captures better the hard transitions between the two facies. To illustrate this last point visually, Fig. 4 shows the best k-term approximation of our target image adopting the DCT and the Haar Wavelet (DB1).

When we incorporate the coherence indicator of the bases, i.e., $\mu(U_j)$ in Eq. (12), to address the basis selection (BS) in Eq. (15), the balance completely changes in favor of the DCT. In particular, Fig. 6 shows the RHS of Eq. (15) and its trend for different wavelet bases and fidelity values $1/\epsilon$ in a wide range of approximation errors $\epsilon > 0$. We can see that the gain in compressibility shown in Fig. 5 does not compensate the fact that wavelet bases are not sufficiently incoherent with respect to the pixel domain, compared with the DCT, which is almost perfectly incoherent with respect to the pixel domain, see Table 1. Consequently, subject to the pixel-based acquisition scheme of Section 3, by far the DCT is the best basis from the point of view of solving our BS problem in (15) and, equivalently, from the point of view of taking advantage of the pixel measurements. In conclusion, the DCT is the basis that will

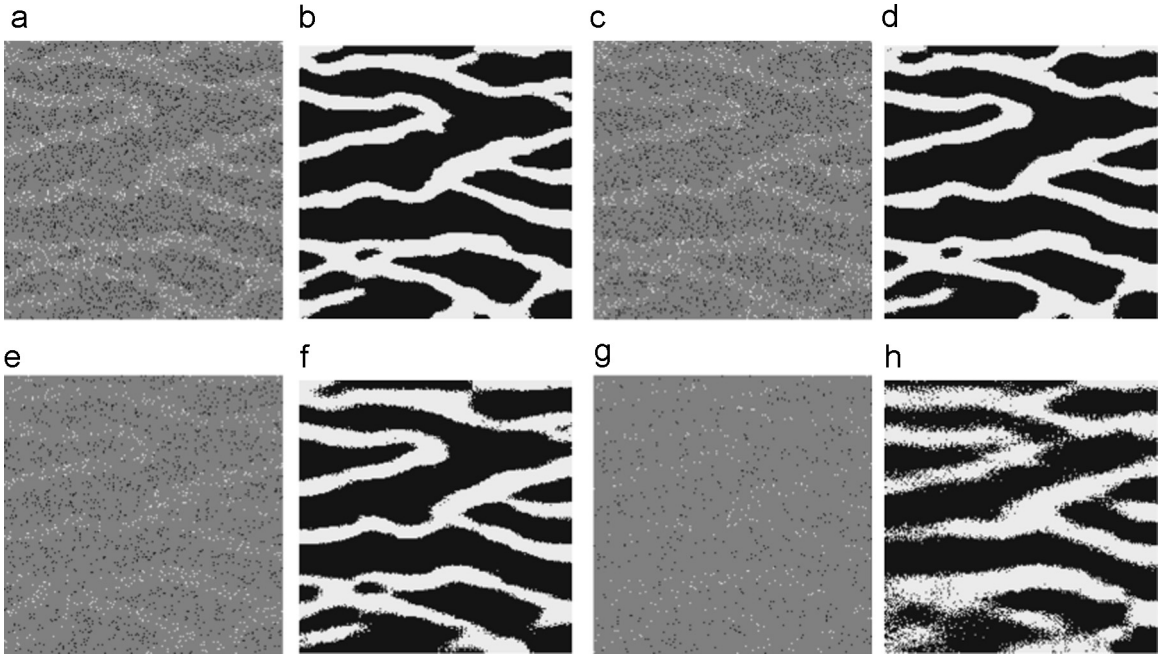

Fig. 12. Average reconstruction across block sizes with different proportion of measurements. (a) and (b) show the 10% of the data and the reconstruction, respectively. (c) and (d) show the same graphics for 8% of data. (e) and (f) for the 5%. (g) and (h) for the 2%.

be considered for the CS reconstruction experiments conducted in the following section.

6. Reconstruction results

In this section reconstruction results are presented and analyzed. The multiple point simulation algorithm `snesim` developed in `SGeMS` (Strebelle, 2002; Remy et al., 2009) is used to create a rich collection of multichannel fields of arbitrary complexity and size. In particular, one hundred images of 200×200 pixels (pp) are created with different structures and orientations, capturing the typical channel structure of the geological phenomenon of interest. A sample of these images is presented Fig. 2. The results obtained with the CS scheme were orientation-invariant, and consequently, we focus on presenting the results applied to images that have left-to-right dominant channel orientation.

6.1. Block decomposition and the average inter-block reconstruction

As the measurements were obtained at random pixel locations with a given proportion (from 1% to 10%), this allows us to decouple the reconstruction by decomposing the image in non-overlapping square-blocks and then applying the ℓ_1-minimizer in Eq. (10) individually in each block (see Fig. 7(c)–(g)). On average, each resulting sub-image will have a similar number of pixels by the nature of the random sensing modality in Eq. (9). This has an important algorithmic advantage, because it reduces the complexity of the reconstruction that scales from $O(n \log n)$ to $O((n \log n)/k)$ (Kunis and Rauhut, 2008; Elad, 2010), n being the size (number of pixels) of the image and k being the number of blocks, allowing the framework to handle very large images. On the negative side, this approach introduces block-wise artifacts, see Fig. 7(c)–(g). However, we will see that this can be compensated in the process of averaging the information across different block sizes, see Fig. 7(h).

Moving to the experimental setting, we took random pixels with different proportions in the range of 1–10% of the size of the image. From these data, we applied the block-by-block ℓ_1-minimizer CS reconstruction presented in Section 3 considering different block sizes (from 40×40 pp to 200×200 pp). Fig. 7 shows the reconstructions of an image with 5% of measurements considering different block sizes organized from left-to-right. We also provide the average reconstruction across all the block sizes that is shown in Fig. 7(h). Finally in all these scenarios, we adopted a two-level hard thresholding as the final post-processing stage. The objective of this final quantization is to match the categorical nature of the facies images. For that, we consider an adaptive threshold (applied pixel-wise on the continuous image provided by the CS scheme) that preserves the proportion of white and black points observed in the direct measurements.

From the results illustrated in Fig. 7, it is possible to see that by increasing the block size of the reconstruction, better image quality is obtained at the expense of increasing the complexity of the ℓ_1-decoding algorithm. A simple justification is that the artifacts induced by connecting non-overlapping reconstructions are reduced in this process. A more fundamental reason is that by increasing the size of the block, the image becomes more compressible with respect to the DCT. Consequently with the same measurements, more image structure in terms of compressibility can be incorporated in the ℓ_1-recovery process (Corollary 1). This compressibility trend is shown in Fig. 8, where the k-best approximation errors, measured in terms of $10 \log \|x\|_{l2}/\sigma_s(x)_{l2}$ (a relative approximation error), are presented as a function of the number of significant coefficients and the size of the block.

Supporting the results in Fig. 8, the difference between the reconstruction $\hat{x}$ and the real images x is computed in the signal to noise ratio (SNR) sense (using the classical expression $10 \log \|x\|_{l2}/\|\hat{x} - x\|_{l2}$ in dB), and also the well-adopted index of perceptual similarity (the structured similarity index (SSIM)) (Zhou et al., 2004) used to evaluate the quality of state-of-the-art image compression techniques. Figs. 9 and 10 show these results as a function of the block size and the number of measurements from 1% to 10% of the total image data. Both in terms of SNR and SSIM, there is a clear performance improvement by increasing the block size, in particular by passing from 40×40 pp to 70×70 pp the gain is important in the whole range from 1% to 10% of the

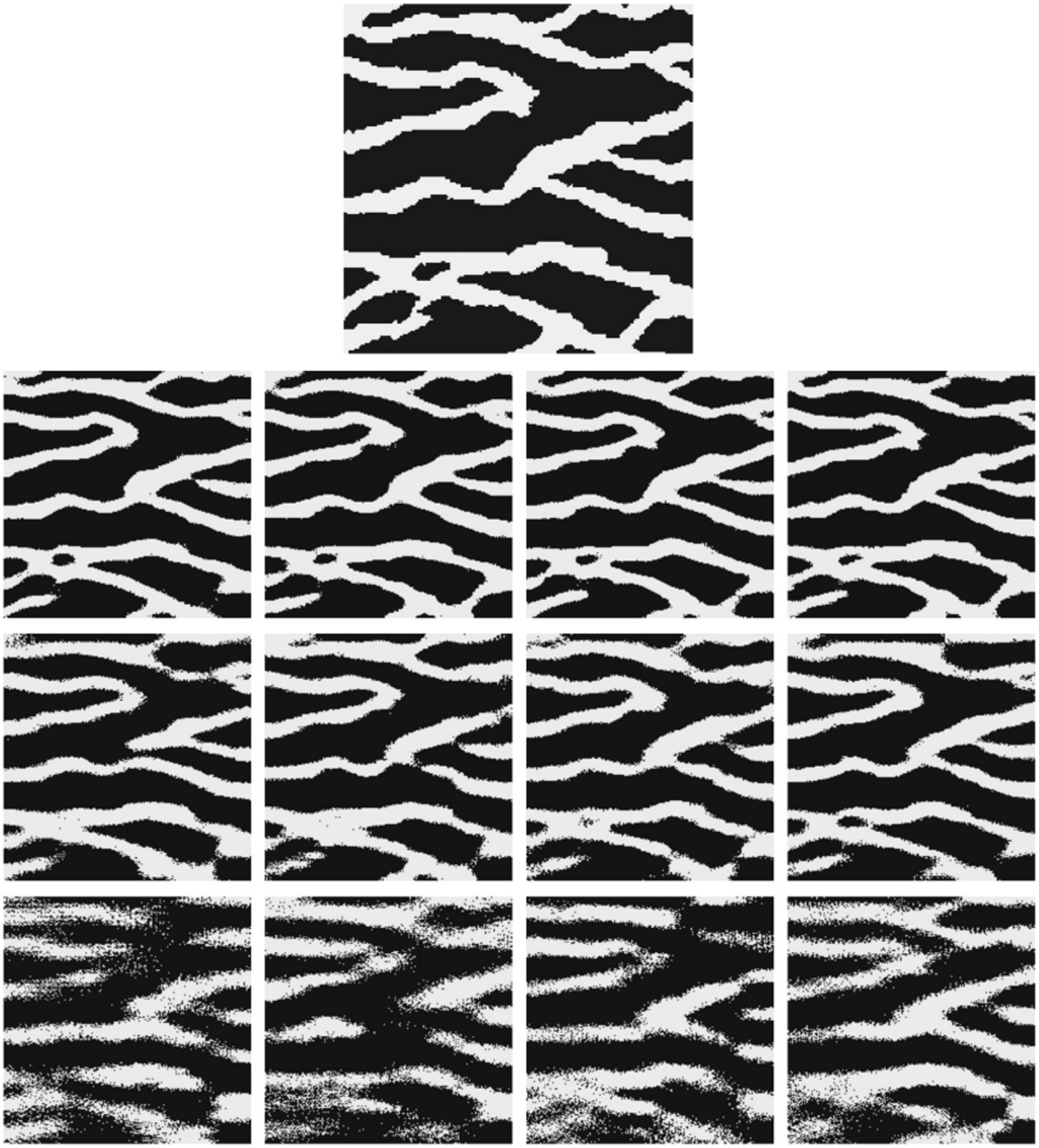

Fig. 13. Illustration of the sensing variability of the CS reconstruction. Four independent reconstructions are presented (organized by columns), in the regime of 10%, 5% and 2% of direct data (organized in rows from top to bottom), respectively. The original image is presented at the very top.

measurements. In addition, these figures show the results without and with the adaptive hard-thresholding, where it is clear that thresholding improves performances. In particular for the best scenario of the average reconstruction the gain is significant. To illustrate this result, Fig. 11 shows examples of continuous versus categorical reconstructions.

From the results in Figs. 9 and 10, we notice a dramatic improvement when adopting the average image reconstruction, in particular in the regime from 2% to 6% pixel measurements and in conjunction with the hard-thresholding post-processing. It is worth noting the improvement in terms of SSIM in Fig. 10, which is aligned with the human perception of the image quality. Hence, the average reconstruction (see Fig. 7(h)) significantly increases the quality of the recovered image when compared with its individual block-by-block recoveries (see Fig. 7(c)–(g)). This can be attributed to the fact that averaging helps compensating the artifacts of the block-by-block processing. However, we believe that the major gain comes from the multi-scale nature of this approach, because in the process of averaging information across blocks of different sizes (from 40×40 pp to 200×200 pp), there is a persistent pattern across scale that provides the performance boost.

Finally for the best setting (average reconstruction with hard-thresholding), Fig. 12 shows the recovered images and the actual data in four sample regimes. First, it is evident the perceptual accuracy of the method when more than 5% of the data is available. What is more interesting is that even with 2% of unstructured data, we can recover an image that is acceptable in terms of preserving the channel structures of the original image, which makes this framework very attractive for image reconstruction and an interesting complement to state-of-the-art simulation-based techniques.

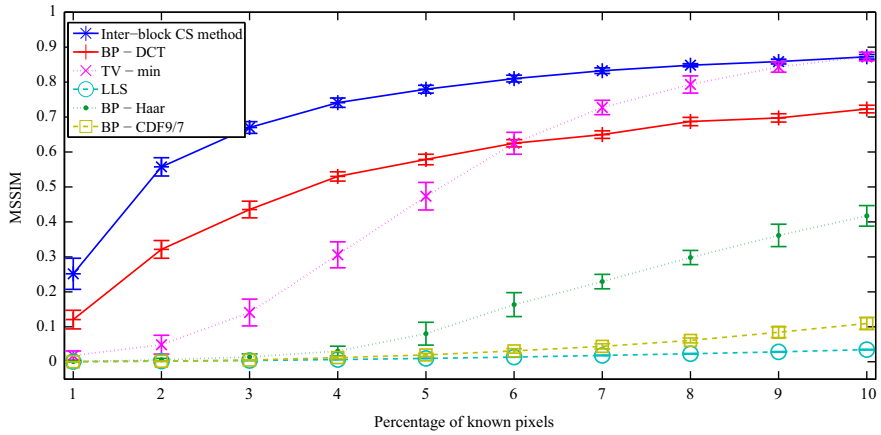

Fig. 14. Average performance and standard deviation of the proposed CS scheme (inter-block CS method), the basis pursuit with the DCT (BP-DCT), the BP with a Haar basis (BP-Haar), BP with the CDF9/7 basis (BP-CDF9/7), total variation minimization (TV-min), linear least square (LLS). Performances obtained for 15 realizations of the sensing matrix and using SSIM as image quality indicator.

6.2. Analysis of the sensing variability and comparison with other methods

As the sensing matrix A is random, it is of interest to analyze the variability in the reconstruction when considering a collection of sensing matrices generated by the random sensing approach in Section 3. A key question to ask is: how much do the results deviate from the average performance? In other words, we want to evaluate the robustness of the CS method given the random nature of A.

In addition, we use this analysis to compare our best CS based solution, with other signal processing (interpolation) techniques. On this, we applied the classical basis pursuit (BP) algorithm (Candès, 2008; Candès et al., 2006a,b; Elad, 2010) on the whole image using the DCT (as explored in Jafarpour et al., 2009), the Haar basis with 5 levels of iterations (Vetterli and Kovacevic, 1995), and the bi-orthogonal Wavelet CDF9/7 (Cohen et al., 1992) with 5 level of iterations (used for image compression in JPEG2000, Wallace, 1991; Vetterli and Kovacevic, 1995). Furthermore, we explore two other regularized solutions for ill-posed image reconstruction: the total variations (TV) minimization (subject to linear measurements) (Needell and Ward, 2013; Lee and Kitanidis, 2013), and the linear least square (LLS) (Elad, 2010, Chapter 1.1) (also explored in Jafarpour et al., 2009).

Concerning robustness, we fix the channel images in Fig. 7(a), and run our best inter-block average CS reconstruction with the adaptive hard-thresholding for 25 independent realizations of A in Eq. (9) preserving the same number of measurements across the scenarios. To illustrate the results, Fig. 13 provides solutions for different proportions of measurements (organized by rows from 10% to 2%) and showing four independent reconstructions (organized by columns). These examples illustrate the robustness of the CS method in the range above 5% of measurements, in the sense that the recoveries are almost invariant to the specific realization of A, see Fig. 14(b). On the other hand, in the critical range of [1–4%], examples in the last row of Fig. 13, the variability increases, because the limited data could result in blocks that are under-represented, from instance to instance of the sensing matrix A, and consequently this translates in higher uncertainty. In other words, the deviation with respect to the average performance value, as expected, tends to increase by considering smaller fraction of the data. This is shown in Fig. 14 where average performance (MSSIM) and the respective standard deviation are reported.

Concerning the trend in performance presented for all the methods in Fig. 14, our CS method offers better reconstruction results in all data-rate regimes, which is clear for rates in [1–6%]. There is clear gain with respect to the more competitive pure BP with the DCT basis, showing the importance of the proposed inter-block averaging process and the adaptive hard-thresholding. When comparing results within the family of BP solution, we can ratify the quality of the DCT in terms of performance in all the range [1–10%]. Bases known to have better compressibility than the DCT (like the CDF9/7 and the Haar bases) do not translate that compressibility gain into the CS reconstruction. The RIPless CS theory offers an explanation for this (Section 3), because incoherence with the pixel-based domain plays a more important role as showed in Sections 4 and 5. On the other hand, the TV minimization approach shows to be an attractive alternative when more than 8% of data is available, which is better than the plain use of BP with the DCT. Finally, the non-sparsity promoting solution (LLS) shows the poorest results in all the data-rate regimes.

7. Summary and final discussion

This work investigates the problem of facies reconstruction from under-sampled data (the regime from 1% to 10%) without the use of a training image. This is an alternative to the way prior information has been modeled and incorporated for this recovery problem in geostatistics. A key contribution is the way in which this problem is put on the framework of compressed sensing (CS). A bridge between the well-elaborated RIPless CS theory and practical aspects of this recovery problem is provided. From this bridge, the basis selection problem is addressed where a justification that the DCT is an excellent alternative for the recovery of facies is presented. On top of that, a new inter-block averaging process and an adaptive hard-thresholding method are proposed, which offer a significant boost in performances in the regime of 1–10% of direct data. Interestingly, this approach shows that the objective of true facies reconstruction is feasible, when we have access to a critical number of measurements in the range of [3%, 5%]. On the other hand, good reconstructions are reported even when less than 3% of the hard-data is available, which is known to be a very challenging problem. Hence, we can say that this CS based approach is able to recover geological facies images from scatter data with no small scale information, which is precisely the regime where the direct sampling method presents some difficulties (Mariethoz and Renard, 2010).

This CS approach offers promising new avenues for geological image reconstructions, and we believe that much work needs to be done to address the relevant scenario with less than 1% of data, where this signal processing approach begins to show clear

limitations, see Fig. 11. One important direction is to jointly incorporate signal structural information (in the CS paradigm) as well as (multiple-point) statistical information from a training image, as conventionally used in geostatistics. In this direction, it is worth mentioning some new results in the context of subsurface model calibration based on nonlinear (dynamic) flow data (Khaninezhad et al., 2012; Elsheikh et al., 2013; Khaninezhad and Jafarpour, 2014). They have explored the idea of integrating a prior geologic model to create a specialized geologic dictionary that is used to reconstruct images from non-linear measurements with good results. This is an interesting alternative to explore in our linear sampling context, however, the specific challenges of our problem need to be considered. For instance, the random nature of the sensing modality, and the fact that good bases relay not only on compressibility as in Khaninezhad et al. (2012) and Elsheikh et al. (2013), but on a formal trade-off between compressibility and coherence.

Acknowledgments

The work is supported by the research grant Fondecyt 1140840, CONICYT, Chile and the Basal AMTC center. We are grateful with Dr. Claudio Estevez and Cesar Azurdia for proofreading this material.

References

Arpat, B., Caers, J., 2007. Conditional simulations with patterns. Math. Geol. 39 (2), 177–203.
Blumensath, T., Davies, M., 2009. Iterative hard thresholding for compressive sensing. Appl. Comput. Harmon. Anal. 27 (November (7)), 265–274.
Candès, E., 2008. The restricted isometry property and its applications for compressed sensing. C. R. Acad. Sci. Paris I 346, 589–592.
Candès, E., Plan, Y., 2011. A probabilistic and RIPless theory of compressed sensing. IEEE Trans. Inf. Theory 57 (11), 7235–7254.
Candès, E., Romberg, J., Tao, T., 2006a. Robust uncertainty principles: exact signal reconstruction from highly incomplete frequency information. IEEE Trans. Inf. Theory 52 (2), 489–509.
Candès, E., Romberg, J., Tao, T., 2006b. Stable signal recovery from incomplete and inaccurate measurements. Commun. Pure Appl. Math. 59, 1207–1223.
Candès, E., Tao, T., 2005. Decoding by linear programming. IEEE Trans. Inf. Theory 51 (December (12)), 4203–4215.
Candès, E., Tao, T., 2006. Near-optimal signal recovery from random projections: universal encoding strategies?. IEEE Trans. Inf. Theory 52 (December (12)), 5406–5425.
Cohen, A., Dahmen, W., DeVore, R., 2009. Compressed sensing and best *k*-term approximation. J. Am. Math. Soc. 22 (July (1)), 211–231.
Cohen, A., Daubechies, I., Feauveau, J., 1992. Biorthogonal bases of compactly supported wavelets. Commun. Pure Appl. Math. 45 (5), 485–560.
Daubechies, I., 1988. Orthonormal bases of compactly supported wavelets. Commun. Pure Appl. Math. 41, 909–996.
Donoho, D., 2006. Compressed sensing. IEEE Trans. Inf. Theory 52 (4), 1289–1306.
Donoho, D.L., Vetterli, M., DeVore, R.A., Daubechies, I., 1998. Data compression and harmonic analysis. IEEE Trans. Inf. Theory 44 (6), 2435–2476.
Elad, M., 2010. Sparse and Redundant Representations, 1st ed. Springer, New York.
Elsheikh, A., Wheeler, M., Hoteit, I., 2013. Sparse calibration of subsurface flow models using nonlinear orthogonal matching pursuit and an iterative stochastic ensemble method. Adv. Water Resour. 56, 14–26.
Guardiano, F., Srivastava, M., 1993. Multivariate geostatistics: beyond bivariate methods. In: Geostatistics-Troia. Kluwer Academic, Amsterdam, pp. 133–144.
Herrmann, F.J., Friedlander, M.P., Yilmaz, O., 2012. Fighting the curse of dimensionality: compressive sensing in exploration seismology. IEEE Signal Process. Mag. 29, 88–100.
Herrmann, F.J., Li, X., 2012. Efficient least-squares imaging with sparsity promotion and compressive sensing. Geophys. Prospect. 60, 696–712.
Jafarpour, B., 2011. Wavelet reconstruction of geologic facies from nonlinear dynamic flow measurements. IEEE Trans. Geosci. Remote Sens. 49 (5), 1520–1535.
Jafarpour, B., Goyal, V.K., McLaughlin, D.B., Freeman, W.T., 2009. Transform-domain sparsity regularization for inverse problems in geosciences. Geophysics 74 (September–October (5)), R69–R83.
Jafarpour, B., Goyal, V.K., McLaughlin, D.B., Freeman, W.T., 2010. Compressed history matching: exploiting transform-domain sparsity for regularization of nonlinear dynamic data integration problems. Math. Geosci. 42 (1), 1–27.
Jafarpour, B., McLaughlin, D.B., 2009. Reservoir characterization with the discrete cosine transform. SPE J. 14 (1), 182–201.
Khaninezhad, M.M., Jafarpour, B., 2014. Hybrid parametrization for robust history matching. SPE J. 19 (3), 487–499.
Khaninezhad, M.M., Jafarpour, B., Li, L., 2012. Sparse geologic dictonaries for subsurface flow model calibration: part 1 inversion formulation. Adv. Water Resour. 39, 106–121.
Kunis, S., Rauhut, H., 2008. Random sampling of sparse trigonometric polynomials, ii. orthogonal matching pursuit versus basis pursuit. Found. Comput. Math. 8 (6), 737–763.
Lee, J., Kitanidis, P., 2013. Bayesian inversion with total variations prior for discrete geologic structure identification. Water Resour. Res. 49, 7658–7669.
Leuangthong, O., McLennan, J., Deutsch, C., 2004. Minimum acceptance criteria for geostatistical realizations. Nat. Resour. Res. 13 (September (3)), 131–141.
Mallat, S., 2009. A Wavelet Tour of Signal Processing, 3rd ed. Academic Press.
Mallat, S., Zhang, Z., 1993. Matching pursuit with time–frequency dictionaries. IEEE Trans. Signal Process. 41 (December (12)), 3397–3415.
Mariethoz, G., Lefebvre, S., 2014. Bridges between multiple-point geostatistics and texture synthesis: review and guidelines for future research. Comput. Geosci. 66, 66–80.
Mariethoz, G., Renard, P., 2010. Reconstruction of incomplete data sets or images using direct sampling. Math. Geosci. 42, 245–268.
Needell, D., Ward, R., 2013. Stable image reconstruction using total variation minimization. SIAM J. Imaging Sci. 6 (2), 1035–1058.
Nyquist, H., 1928. Certain topics in telegraph transmission theory. Trans. AIEE 47 (April (2)), 617–644.
Ortiz, J.M., Deutsch, C.V., 2004. Indicator simulation accounting for multiple-point statistics. Math. Geol. 36 (5), 545–565.
Peredo, O., Ortiz, J.M., 2011. Parallel implementation of simulating annealing to reproduce multiple-point statistics. Comput. Geosci. 37, 1110–1121.
Remy, N., Boucher, A., Wu, J., 2009. Applied Geostatistics with SGeMS, A User's Guide. Cambridge University Press.
Shannon, C.E., 1949. Communication in the presence of noise. Proc. IRE 37 (January (1)), 10–21.
Starck, J.-L., Murtagh, F., Fadili, J.M., 2010. Sparse Image and Signal Processing. Cambridge University Press.
Strebelle, S., 2002. Conditional simulation of complex geological structures using multiple points statistics. Math. Geol. 34 (1), 1–22.
Tahmasebi, P., Sahimi, M., Caers, J., 2014. Ms-ccsim: accelerating pattern-based geostatistical simulation of categorical variables using multi-scale search in Fourier spaces. Comput. Geosci. 67, 75–88.
Tan, X., Tahmasebi, P., Caers, J., 2014. Comparing training-image based algorithms using an analysis of distances. Math. Geosci. 46, 149–169.
Tropp, J., Gilbert, A., 2007. Signal recovery from random measurements via orthogonal matching pursuit. IEEE Trans. Inf. Theory 53 (December (12)), 4655–4666.
Vetterli, M., Kovacevic, J., 1995. Wavelet and Subband Coding. Prentice-Hall, Englewood Cliffs, NY.
Wallace, G.K., 1991. The jpeg still picture compression standard. Commun. ACM 34 (April), 30–44, URL: ⟨http://doi.acm.org/10.1145/103085.103089⟩.
Wu, J., Boucher, A., Zhang, T., 2008. A SGeMS code for pattern simulation of continuous and categorical variables: FILTERSIM. Comput. Geosci. 34 (12), 1863–1876.
Zhou, W., Bovik, A., Sheikh, H., Simoncelli, E., 2004. Image quality assessment: from error visibility to structural similarity. IEEE Trans. Image Process. 13 (4), 600–612.